Pose-Angular Tracking of Maneuvering Targets With High Range Resolution (HRR) Radar

Chun Yang
Sigtem Technology, Inc.
San Mateo, CA 94402
chunyang@sigtem.com

Erik Blasch
Air Force Research Lab
WPAFB, OH 45433
erik.blasch@wpafb.afb.mil

Abstract – Ground targets are constrained on the Earth with their velocity vector direction aligned mostly along the body longitudinal axis. The pose angle therefore carries kinematic information useful for tracking maneuvering targets. For target identification (ID), range profiles obtained by a high range resolution (HRR) radar are compared with reference templates in pose angle per target class, thus producing pose angle estimates. In this paper, we present a method for measuring the pose angle of a maneuvering target by first converting the matching scores of a classifier into a "likelihood" function and then updating the likelihood function probabilistically. By accumulating the likelihoods of possible poses over time, it enables the pose angular tracking as the target is undertaking turn maneuvers. Simulation results for pose angular tracking are presented wherein range profiles are generated from RF signatures of moving targets.

Keywords: Tracking, Maneuver, Target ID, Pose, HRR.

1 Introduction

Compared to conventional tracking with post-detection observables such as range, range rate, and bearings, feature-aided tracking (FAT) works on low-level measurements. When compared with reference templates in a database, a successful matching provides target type and viewing angles (or pose angles) among others. It thus offers an extended target state including not only the kinematic variables such as position, velocity, and possibly acceleration but also the target's orientation relative to its environment (terrain and road).

For an HRR radar [14], range profile is a one-dimensional (1D) measurement of target radar reflectivity along the radar to target line of sight (LOS) vector where the amplitudes are statistical features. This look vector, when expressed in the target body frame in terms of the aspect and depression angles, is called a "pose." For practical reasons, a target is pre-sampled into a template library of range profiles at discrete poses. A successful template matching therefore identifies the target type and at the same time produces the pose at which the range profile is generated.

HRR range profiles have long been used for target identification (ID) or fingerprinting [8, 9, 13, 15]. It has also been used in data association to improve track continuity [3, 6]. Recently, the pose angular measurements as a by-product of target ID have been used to assist target tracking [16]. It exploits the fact that ground targets are constrained to move on the Earth surface and their velocity vector direction is aligned mostly along the body longitudinal axis. The pose angle therefore carries kinematic information which is particularly helpful and fast about target maneuvers.

The angular pose of a target is typically estimated in two ways. One way is to consider the target pose as an intermediate result or a by-product (a nuisance parameter) of the target ID process as described above. A template must have about the same pose angles (azimuth and elevation, aspect and depression) as the target in order to reach a successful classification. Target pose is used as a search parameter in the target ID process.

In the second way, target pose is estimated explicitly for a target with known ID. For example, neural networks were used for pose estimation with for HRR and SAR images [7, 11] where the weight vector is obtained through training.

It is well known that 1D HRR signatures are subject to high variability due to scintillation effects (speckles). That is, multiple scatterers fallen in a single range bin interact either constructively or destructively when the aspect angle is changed slightly. This is the basis for rather sensitive pose estimation. In conventional classifier designs, the sensitivity to pose angles is minimized so that few templates are required to discriminate between different classes of targets. However, in classifier-based pose angular estimation, we would like to maximize the sensitivity of a classifier to pose angles.

In this paper, a particular classifier, namely, the MTE algorithm [4], is used for pose estimation. Due to the discrete nature of reference templates and errors in range profiles, the pose angular estimate is not single-valued but rather is a distribution of matching scores at the output of a classifier. In this paper, we present a method for measuring the pose angle of a maneuvering target by first converting the matching scores of a classifier into a "likelihood" function and then updating the likelihood function probabilistically. By accumulating the likelihoods of possible poses over time, it enables the pose angular tracking as the target turns.

The paper is organized as follows. In Section 2, the MTE classification algorithm is first described. In Section 3, pose angular estimation with the MTE classifier is detailed together with simulation results presented to illustrate the

			Form Approved OMB No. 0704-0188

Report Documentation Page

1. REPORT DATE **JUL 2008**	2. REPORT TYPE	3. DATES COVERED **00-00-2008 to 00-00-2008**

4. TITLE AND SUBTITLE **Pose-Angular Tracking of Maneuvering Targets With High Range Resolution (HRR) Radar**	5a. CONTRACT NUMBER
	5b. GRANT NUMBER
	5c. PROGRAM ELEMENT NUMBER
6. AUTHOR(S)	5d. PROJECT NUMBER
	5e. TASK NUMBER
	5f. WORK UNIT NUMBER

7. PERFORMING ORGANIZATION NAME(S) AND ADDRESS(ES) **Air Force Research Laboratory,Wright Patterson AFB,OH,45433**	8. PERFORMING ORGANIZATION REPORT NUMBER
9. SPONSORING/MONITORING AGENCY NAME(S) AND ADDRESS(ES)	10. SPONSOR/MONITOR'S ACRONYM(S)
	11. SPONSOR/MONITOR'S REPORT NUMBER(S)

12. DISTRIBUTION/AVAILABILITY STATEMENT
Approved for public release; distribution unlimited

13. SUPPLEMENTARY NOTES
11th International Conference on Information Fusion, June 30 ? July 3, 2008, Cologne, Germany.

14. ABSTRACT
see report

15. SUBJECT TERMS

16. SECURITY CLASSIFICATION OF:			17. LIMITATION OF ABSTRACT	18. NUMBER OF PAGES	19a. NAME OF RESPONSIBLE PERSON
a. REPORT **unclassified**	b. ABSTRACT **unclassified**	c. THIS PAGE **unclassified**	**Same as Report (SAR)**	**8**	

concept and performance. Section 4 concludes the paper with future work outlined.

2 MTE Method for Range Profile Comparison

There are different classifiers available for matching a measured HRR range profile with reference range profiles in a template database. One method is the linear regression matching algorithm [13]. Another method that is used in this paper is adopted from the DARPA MTE program [4]. The MTE algorithm is a minimum squared error (MSE)-based algorithm. It has the following features. It exhibits a matched-filter behavior, compensates for differences in profile gain, searches over range shifts to find the best profile alignment and includes weighting to increase importance of high-amplitude peaks.

The inputs to the algorithm include a "Target" HRR profile in dB, $\underline{P}$, with a profile mask, $\underline{m}_p$, and a "Template" HRR profile in dB, $\underline{T}$, with a profile mask, $\underline{m}_t$. It further includes an estimated mean clutter value for the target profile, c, a number of range shifts over which to search, N, and a weighting parameter, w.

If the template HRR profile and target HRR profile are given in amplitude, $\underline{p}$ and $\underline{t}$, they will first be converted to the HRR profiles in dB, $\underline{P}$ and $\underline{T}$, respectively. Similarly, the estimated mean clutter value for the target profile in dB, C, is also calculated from amplitude c, which can be estimated from the target profile $\underline{P}$ as the median value of the off-mask pixels. The calculations are given by:

Template profile: $\underline{p} = 10^{\underline{P}/20}$ and $\underline{P} = 20\log_{10}(\underline{p})$ (1a)

Target profile: $\underline{t} = 10^{\underline{T}/20}$ and $\underline{T} = 20\log_{10}(\underline{t})$ (1b)

Mean clutter: $c = 10^{C/20}$ and $C = 20\log_{10}(c)$ (1c)

The MTE algorithm consists of the following steps. In the first step, the template profile in $\underline{T}$ at off-mask range bins is set to the mean clutter C. The second step is to align the profiles in range using the profile masks. The two profiles can be aligned either at the leading edge of the masks or at their centroids. If the two profiles are of different lengths, the unaligned parts are filled with the mean clutter, C. The next step is to calculate a complementary weight vector for the target profile by:

$$\underline{W}_p = \begin{cases} \exp(-10^{(\underline{P}-C)/20}/w) = \exp(-\underline{p}/cw), & P > C, \text{ on-mask} \\ \exp(-1/w), & P \leq C, \text{ on-mask} \\ C, & \text{off-mask} \end{cases} \quad (2)$$

From (2), the complementary weighting $\underline{W}_p$ varies according to the profile amplitude as compared to the mean clutter. Off mask, the weight is assigned a constant value and on mask, when a target profile value is equal to or smaller than the mean clutter, the weight is also constant. When a target profile value is greater than the mean clutter, its ratio with the mean clutter is taken as the exponent of a negative exponential, and the resulting complementary weight is rather small.

The next step is to shift the template profile, adjust its gain, and calculate its weight prior to comparing it with the target profile. There will be 2N+1 shifts from –N to N. This is done by the following loop:

For $s = -N$ to N:

- Shift $\underline{T}$ in range by s range bins.
- Compute the average difference between $\underline{T}$ and $\underline{P}$ over the intersection of their masks for value above the mean clutter C to obtain the optimal gain adjustment.
- Adjust $\underline{T}$ by biasing it with the average difference (addition in dB is equivalent to scaling in amplitude in the optimal gain).
- Compute the weighting $\underline{W}_t$ using the same formula as in (2) for the gain adjusted template $\underline{T}$.
- Compute the combined weight as:

$$\underline{W} = 1 - \underline{W}_t \circ \underline{W}_p \quad (3)$$

  where $\circ$ stands for element to element multiplication of two vectors.

- Compute the MTE score for this shift as:

$$Score(s) = \frac{\sum \underline{W} \circ (\underline{P} - \underline{T})^2}{\sum \underline{W}} \quad (4)$$

  where the summations are carried out over the vector elements and the summation in the denominator is over those bins with value over c.

End

The final MTE score is computed as:

$$MTE = \min_s Score(s) \quad (5)$$

Since the score is marked by the total distance between the two profiles, more importance (large weight) is placed on characteristic bins. In other words, the profile values at those bins have to be close, otherwise, they weight up the cumulative differences between the two profiles.

3 Pose Angular Estimation with MTE

The MTE classifier output is also called the MTE discriminant or discriminant for short and will be analyzed in this section. Two methods for angular estimation are then described.

3.1 MTE Classifier Discriminant Analysis

The range profiles of two targets, i.e., a generic tank and a vehicle transport, are generated with the simulation environment shown in Fig. 1. It consists of the Simulation Tool for Advanced Radar Systems (STARS), developed by ATK Mission Research (Dayton, OH) [12] and the Radar Signature Predictor (SigPred), developed by General Dynamics Advanced Information Systems (Ann Arbor, MI) under the Air Force program Feature-Aided Tracking of Stop-move Objects (FATSO) [10]. More information about the simulation environment can be found in [18, 19].

In our simulation, the radar platform is at an altitude of 5000 meters at a constant speed of 100 m/s. The radar sensor is side looking at a fixed depression angle of 12

degrees. The center frequency is 10 GHz with a bandwidth of 600 MHz and the pulse repetition frequency is 2000 Hz.

The discriminant provides a measure of the "distance" between the test profile and the template profile. The smaller the discriminant output or the score, the closer the two profiles look alike. Figs. 2 and 3 show the discriminator outputs where the test profile and the reference templates are for the same target (*i.e.*, auto correlation) for a generic tank and a vehicle transport, respectively. The cross correlation between the two is shown in Fig. 4. To generate these plots, the target is sampled in azimuth in a one-degree increment over 360 degrees. In the auto correlation cases, the test azimuth angles are off the template azimuth angles by 0.2 degrees.

From Fig. 2, the high correlation exists for azimuth angles θ and 360-θ, a longitudinal symmetric. This shows up as the diagonal and anti-diagonal components, a big X. We can also see some minor correlations at angles 180–θ and 180+θ, which form a big O. The minor correlation is less obvious as O in Fig. 3 but rather more like small x. There are also weak correlation features around the plot.

There are no distinct features in Fig. 4 for cross correlation between generic tank and vehicle transport except wide horizontal strips at 90 and 270 degrees, indicating the two targets are difficult to discriminate when viewed from those azimuth angles (broad side). Overall, the vehicle transport seems to be easier than the generic tank for classification and pose estimation.

The discriminant outputs at six consecutive azimuth angles are shown in Fig. 5 for the vehicle transport where the true target azimuth angle varies from 45 to 50 degrees. The target range profile at each azimuth is compared with the set of templates from 0 to 359 degrees but only the first 180 results are plotted. The discriminant values (the distance between the test profile and the template file) are the lowest around the true azimuth angle. There is a secondary dip around 95 degrees due to minor symmetry.

Fig. 6 is the blow-up of Fig. 5 around the dips. When the index of the lowest dip is used as the pose estimates (see Section 3.2 for further discussion), the angular estimation at some azimuth will develop errors. Also note that the discrimination curves do not have the same slopes, some are steeper than others. Besides, the left and right slopes are not symmetric. Those azimuth angles that produce steep discrimination curves can be estimated to a better accuracy.

In summary, when the MTE algorithm is used for pose estimation via search, the discriminant output exhibits certain azimuth symmetry. This includes left vs. right (symmetry about longitudinal axis), front vs. back (symmetry about the perpendicular axis), and some local symmetries. In addition, the discriminant output is volatile (large variations in the score values as a function of azimuth angle) and peaks do not have regular shapes.

The ambiguity due to symmetry may be solved by the target velocity vector, road direction, and sensor to target geometry. The search interval in azimuth may be restricted to a small sector. However, there is a need to consider target maneuver, which can change heading rather quickly particularly over a long sampling interval. Several pose estimation algorithms are presented below.

3.2 Discrete Pose Estimate at Minimum Distance

The discriminant typically does not show a clear winner over a search interval. Therefore, there are several possible ways to obtain an estimate:

- Consider the angular estimate being the search angle that produces the smallest score (*i.e.*, the minimum distance). One way to characterize the estimation error is to use a confusion matrix in much the same way the confusion matrix is used to characterize a classifier.

- Provide a list of discrete estimates being the search angles for the first few smallest scores, together with their respective figure of merit. This is an extension of the first estimation method.

- Generate a distribution over the search interval as the probability that each search angle being the true pose. This provides a likelihood function that can be used in Bayesian reasoning.

For the first method, the search angle that produces the smallest score is taken as the pose estimate. When the index of the lowest dip is searched over 360 degrees in azimuth for the vehicle transport, most estimates lie along the true azimuth angle. However, there are some large excursions between the two symmetric axes. When the search is restricted within 180 degrees in azimuth, thus eliminating the symmetry, the pose angular estimates are shown in Fig. 7. Except for infrequent spikes of a dozen of degrees due to minor symmetry, the rest stays within few degrees. Indeed, except for a large spike of 11 degrees at 84 azimuth angle, other errors are small within 2 degrees. The standard deviation is 1.0826 degrees and 0.6918 degrees after the spike is removed.

For the generic tank, the discriminant output at six consecutive azimuth angles are shown in Fig. 8 where the true target azimuth angle varies from 45 to 50 degrees. The discriminant values are the lowest around the true azimuth angle. Fig. 9 is the shifted and normalized values around the lowest dip. Again, not all dips locate at zero. These normalized discrimination curves do not have the same slopes and the left and right slopes are not symmetric.

Again, when the index of the lowest dip is searched over 360 degrees in azimuth, there are large excursions between the two symmetric axes. The pose angular estimates are shown in Fig. 10 for the search restricted within 180 degrees in azimuth. There is a large excursion at 120 degrees. The rest stays within few degrees of the true angles. Indeed, there are a large spike of 46 degrees at the azimuth angle of 120 degrees and another spike of 13 degrees at the azimuth angle of 100 degrees. Other errors are small within few degrees. The standard deviation is

3.8573 degrees, 1.7656 degrees after the major spike is removed, and 1.4193 degrees if both spikes are removed.

The spikes are caused by the regions near broadside where minor symmetries are present. Although the correct template has a low determinant, another template just happens to be slightly lower, thus creating a pose angular estimation error. It is clear from these figures that the tank is less discriminatory than the vehicle transport, because it has fewer features. The study illustrates the volatility of using a classifier to estimate the pose at some azimuth angles. As shown in [19], near broadside the target may not be visible at all, making the spikes we observe above irrelevant.

3.3 Likelihood Function and Updating

Denote the discriminant output by $\underline{x} = [x(i), i \in \underline{\theta}]^{\mathrm{T}}$ where $x(i) = MTE(\underline{P}, \underline{T}_i)$ over the search angular interval $\underline{\theta}$. Denote the likelihood function by $\underline{y} = [y(i), i \in \underline{\theta}]^{\mathrm{T}}$ where $y(i) = \Pr\{MTE = x | \theta = i\}$. The proposed likelihood function is given by:

$$\underline{y} = a \exp(-\underline{x}/\alpha) \tag{6a}$$

$$a = \sum_{\theta} \exp(-\underline{x}/\alpha) \tag{6b}$$

where a is a normalization factor and α is a weight factor.

This function is designed so as to inverse the score function (a peak rather a dip at a likely azimuth), stretch it (give a larger value to more likely azimuth), and scale it (normalize all into unity). The structure and the factor α of the transform are design parameters.

Consider the state space being the discretized azimuth from 0 to 360 degrees $\underline{\theta}_k$ where k is the time index. Without any specific information about the evolution of $\underline{\theta}_k$ over time, the previous distribution can be used. Instead of working with the pose angle directly, we may choose to work with its distribution over the state space. In this case, the time evolution is characterized by an angular spread matrix, denoted by A, as:

$$A = [A_{ji}] \tag{7a}$$

$$A_{ji} = \Pr\{\theta_{k+1} = j | \theta_k = i\} \tag{7b}$$

$$\sum_{j=0}^{N-1} A_{ji} = 1 \tag{7c}$$

Each entry A_{ji} in the angular spread matrix A prescribes the probability that the true pose at time $k+1$ is j given the true pose at time k is i. The state equation can be written as:

$$\underline{z}_{k+1|k} = A \underline{z}_k \tag{8a}$$

$$z_k = [\Pr\{\theta_k = 0 | X_k\}, \quad \Pr\{\theta_k = \Delta\theta | X_k\}, \quad \cdots$$
$$\cdots \quad \Pr\{\theta_k = \Delta\theta | X_k\}]^T \tag{8b}$$

$$X_k = \{\underline{x}_s, s \le k\} \tag{8c}$$

where $\Delta\theta$ is the angular step used to generate all the templates for search and N is the number of search steps covering the angular uncertainty.

Denote the confusion matrix by C, which defined as:

$$C = [C_{ji}] \tag{9a}$$

$$C_{ji} = \Pr\{\hat{\theta} = j | \theta = i\} \tag{9b}$$

$$\sum_{j=0}^{N-1} C_{ji} = 1 \tag{9c}$$

It prescribes the probability that the discriminant indicates an angular estimate j when the true pose is actually i. The confusion matrix is obtained by running a Monte Carlo simulation of the MTE algorithm over target templates. In a sense, the confusion matrix captures the inherent resemblance or correlation of the target HRR profile as a function of azimuth. This is reflected in the local shape (peaks and valleys) of the discriminant. It also provides a performance figure of merit of a classifier as its sensitivity to the azimuth. Conventional classifier designs actually deemphasize the sensitivity to azimuth by using an averaged template over several degrees of azimuth for instance. In contrast, we seek for a classifier that is sensitivity to azimuth in our application of pose estimation. As a result, the use of confusion matrix C is intended to pick up those distributions that are spread out due to non-orthogonality.

The predicted distribution of the discriminant is:

$$\underline{y}_{k|k-1} = C \underline{z}_{k|k-1} \tag{10}$$

Given the likelihood function $\underline{y}_k$ in (6a), applying the Bayes' formula and the total probability theorem, we obtain a recursive algorithm as:

$$\underline{z}_k = \frac{diag\{\underline{y}_k\}\underline{y}_{k|k-1}}{\underline{y}_k^T \underline{y}_{k|k-1}} = \frac{diag\{\underline{y}_k\}CA\underline{z}_{k-1}}{\underline{y}_k^T CA\underline{z}_{k-1}} \tag{11}$$

The derivation is given as follows. For the true pose $\theta_k = i$, we have

$$z_k(i) = \Pr\{\theta_k = i | X_k\} = \frac{\Pr\{\theta_k = i, \underline{x}_k, X_{k-1}\}}{\Pr\{\underline{x}_k, X_{k-1}\}} \tag{12a}$$

$$= \frac{\Pr\{\underline{x}_k | \theta_k = i, X_{k-1}\}\Pr\{\theta_k = i | X_{k-1}\}\Pr\{X_{k-1}\}}{\sum_j \Pr\{\underline{x}_k | \theta_k = j, X_{k-1}\}\Pr\{\theta_k = i | X_{k-1}\}\Pr\{X_{k-1}\}} \tag{12b}$$

$$= \frac{\Pr\{\underline{x}_k | \theta_k = i\}\Pr\{\theta_k = i | X_{k-1}\}}{\sum_j \Pr\{\underline{x}_k | \theta_k = j\}\Pr\{\theta_k = i | X_{k-1}\}} \tag{12c}$$

$$= \frac{y_k(i)z_{k|k-1}(i)}{\sum_j y_k(j)z_{k|k-1}(j)} = \frac{y_k(i)[CAz_{k-1}](i)}{\sum_j y_k(j)[CAz_{k-1}](j)} \tag{12d}$$

Assembling the expression in (12d) for all elements leads to the vector format in (11).
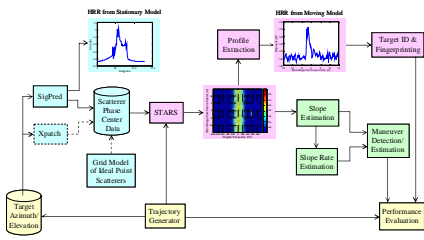
Fig. 1 Simulation Environment with STARS & SigPred (FATSO)
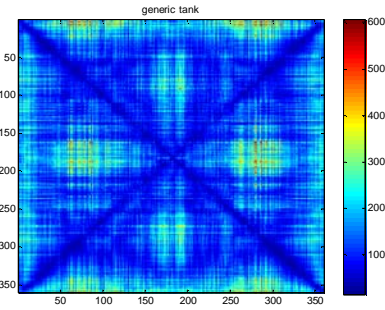

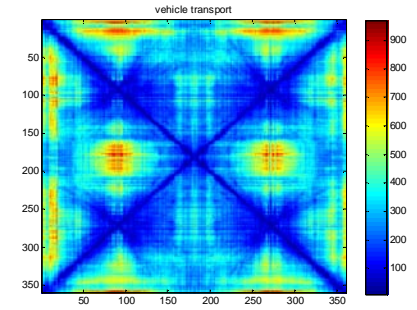
Fig. 2 Discriminator Output for a Generic Tank

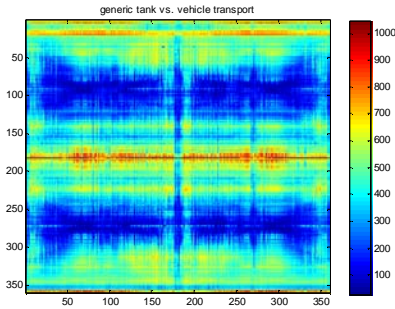Fig. 3 Discriminator for Vehicle Transport

Fig. 4 Discriminator Output for Generic Tank
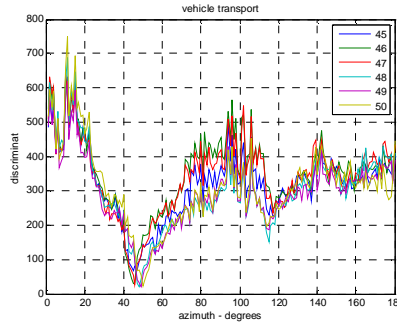

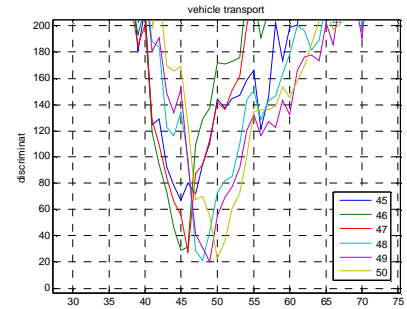Fig. 5 Discriminator at Discrete Azimuth
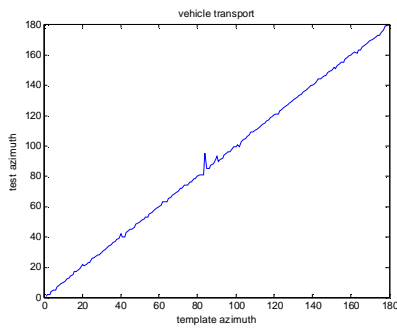

Fig. 6 Discriminator Output (Details)
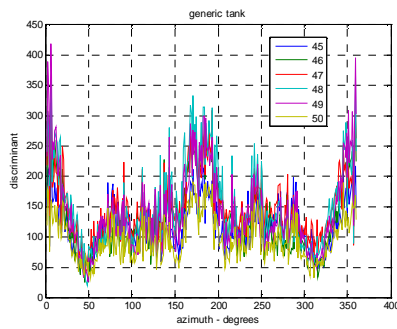

Fig. 7 Dip Index within 180 Degrees

Fig. 8 Discriminator Output at Discrete Azimuth

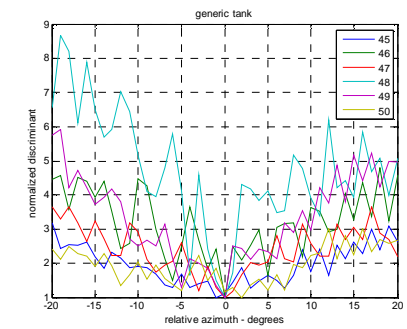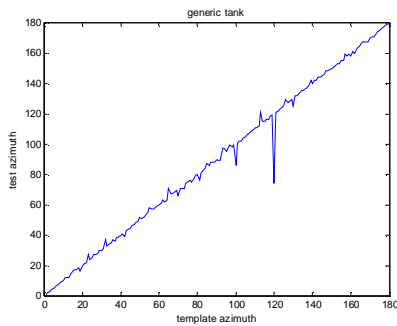Fig. 9 Discriminator (Shifted and Normalized)
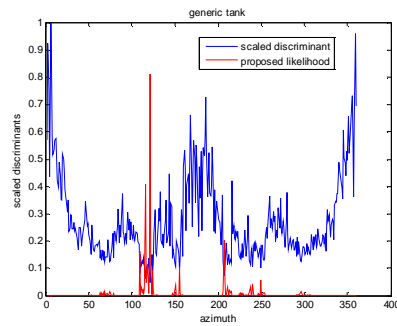

Fig. 10 Dip Index within 180 Degrees

Fig. 11 From Discriminant to Likelihood
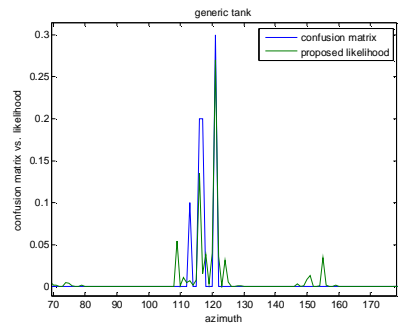
Fig. 12 Confusion Matrix vs. Likelihood

Fig. 11 shows the discriminant outputs (blue-colored) when the template azimuth is varied over 360 degrees for a true pose at 121 degrees. The discriminant is normalized while the proposed likelihood (red-colored) with $\alpha = 8$ is scaled with a factor of 3 so as to display them in the same plot. By exponential stretching and inversing, the dips of the discriminant are transformed into peaks of the likelihood with other values suppressed to around zero.

Fig. 12 shows the 121st row of the confusion matrix (blue-colored) with the corresponding likelihood (green-colored) when the template azimuth is varied from 70 to 180 degrees. The major peaks match quite well between the

two curves with some differences in sidelobes. Noise and clutter contribute to mismatches, which may be averaged out with multiple looks using the recursive algorithm given in (11).

or a similar software program, the azimuth search interval is pre-discretized into a fixed grid. For the fixed azimuth grid points, all templates are calculated off-line. When the pose angle is considered as the state, the state space is also discretized into a fixed grid. The Markov chain, Bayesian rule, and total probability theorem are applied for recursive estimation.

The use of a Markov chain model A to represent the dynamics of pose angular changes may be sufficient if we have enough data (and time) to carry out the recursive computation. In this case with high data rate, the mode filter based on discrete-time point process [17] can be applied. However, except for a dedicated tracking for fire control, the sampling rate is typically low for airborne surveillance applications. An alternative way to track angular pose change is to resort to direct search.

Given a target profile in dB $\underline{P}_k$, the MTE score is calculated against a library of N templates T = [$\underline{T}_\beta$, $\beta = 0$, …, N-1] as:

$$\underline{D}_k = [MTE(\underline{P}_k, \underline{T}_\beta), \quad \beta = 0, ..., N-1]^T \tag{13}$$

The discriminant $\underline{D}_k$ is then converted into the likelihood as defined in (6), rewritten as:

$$\underline{L}_k = LH(\underline{D}_k, \alpha) \tag{14}$$

For two consecutive target profiles in dB $\underline{P}_k$ and $\underline{P}_{k+1}$, we obtain their discriminants $\underline{D}_k$ and $\underline{D}_{k+1}$ using (13) and their likelihoods $\underline{L}_k$ and $\underline{L}_{k+1}$ using (14). It is possible to combine the two measurements using (11) directly. However, a seemly better method is to find the pose change first. This is done by the following search:

$$\omega^* = \max_{\omega \in \Omega}\{\underline{L}_k^T \underline{L}_{k+1}(\omega)\} \tag{15}$$

where ω is the pose angular change in terms of azimuth search steps and Ω is the set of possible pose changes. $\underline{L}_k$ and $\underline{L}_{k+1}$ are then combined using (11) with $A = I$ and $\underline{z}_k = \underline{L}_k$ and $\underline{y}_{k+1} = \underline{L}_{k+1}(\omega^*)$.

Similar filters based on belief theory can also be derived for pose estimation [2].

Consider a generic tank making constant turn with a turn rate of 10 degrees per sampling interval. Six samples are available during the turn of 60 degrees.

Fig. 13 shows the discriminants (*i.e.*, the MTE classifier's output) for the azimuth search angle varied from 0 to 90 degrees in 1 degree increment when the true target is at an azimuth angle of 20, 30, 40, 50, 60, and 70 degrees, respectively. The dip for each curve indicates the estimated target pose azimuth angle.

Fig. 14 shows the transformed discriminants or likelihoods. Clearly, the likelihoods in Fig. 14 provide a

3.4 Pose Angular Tracking

Due to the heavy computation load associated with preparing a target template using the SigPred and STARS

better indication for the pose angle than the discriminants in Fig. 13.

To combine two successive profiles, the likelihood of each new target profile is circularly shifted. The sum of products between the likelihoods of template profile and the shifted target profile is taken for each shift. The optimal shift is the one that produces the maximum for the sums of likelihood products. This optimal shift when scaled by the sampling interval is taken as an estimate of the underlying turn rate. The element by element likelihood products of the template profile and the optimally shifted target profile are normalized to yield the cumulative PDF as shown in Fig. 15. After two and three profile updates (combining), the cumulative PDF tends to become a point mass with probability one.

Fig. 16 shows the estimated shifts vs. the true shifts (a negative/positive value means a left/right shift along the x-axis or an upward/ downward shift of a column vector by the same amount). The average angular error is 0.4 degrees.

Two large errors occurred at the 3rd and 5th shifts, which correspond to the 4th and 6th target profiles. Instead of being peaked, these two profiles are flat around the true azimuth as shown in Fig. 14.

Instead of shifting a target profile, an alternative method is to shift the template profile. Furthermore, the cumulative PDF may be spread with the confusion matrix. This is to prevent a build-up at one particular angular point.

Fig. 17 shows the cumulative PDF obtained using the template shifting (forward combining) and confusion matrix spreading. It is clear that after the confusion matrix spreading, the PDF does not amass at a single point as in Fig. 15.

Fig. 18 shows the estimated shifts vs. the true shifts. The average angular error is 0.4 degrees. Looking at the angular errors for this case does not show any advantage of forward combing because we have a very good estimate at the start.

Now consider a second scenario where we start with an ambiguous estimate. Fig. 19 shows the discriminants for the azimuth search angles over 0 to 90 degrees when the true target is at 50, 60, 70, 80, 90, and 100 degrees, respectively. The dip for each curve indicates the estimated target pose azimuth angle.

Fig. 20 shows the transformed discriminants or likelihoods. Clearly, the likelihoods in Fig. 20 provide a better indication for the pose angle than the discriminants in Fig. 19. As in Fig. 19, the 1st, 3rd, and 5th profile discriminant likelihoods are flat, rather than peaked as for the 2nd and 4th.
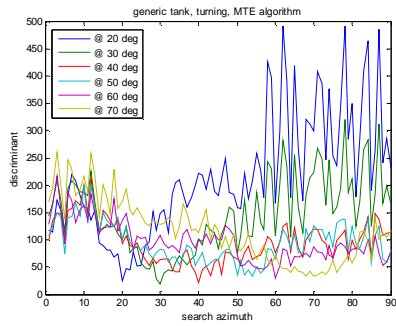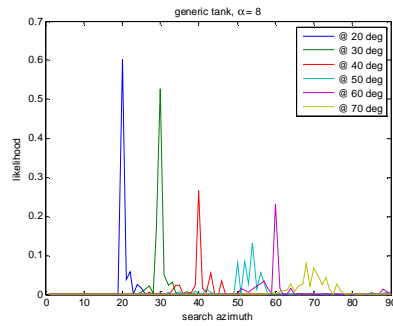
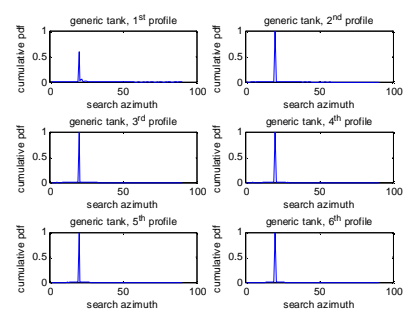Fig. 13 Discriminants

Fig. 14 Likelihoods
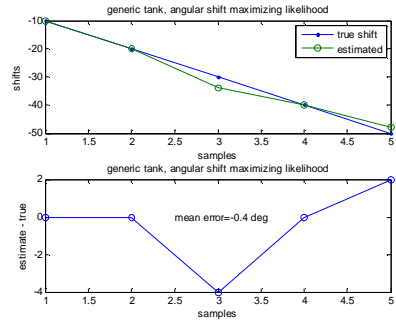

Fig. 15 Cumulative PDF (Backward Combining)

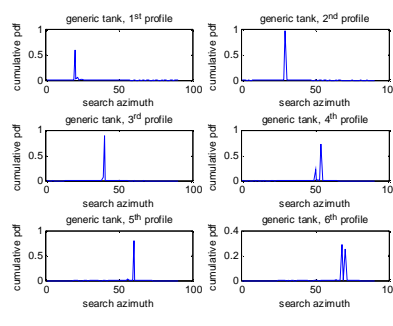Fig. 16 Angular Shift per Sample (Turn Rate)

Fig. 17 Cumulative PDF (Forward Combining)
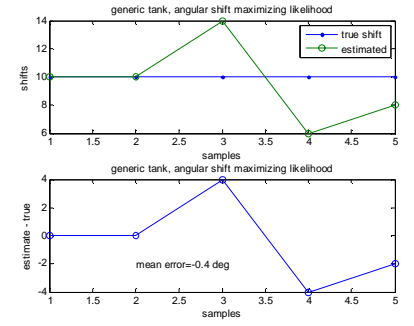

Fig. 18 Angular Shift per Sample (Turn Rate)

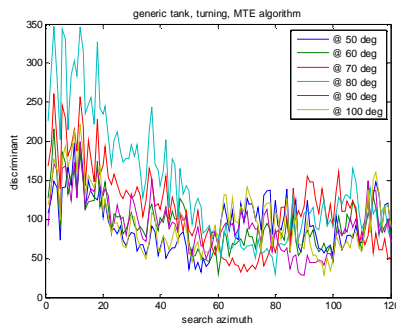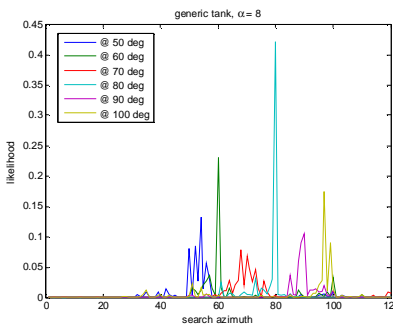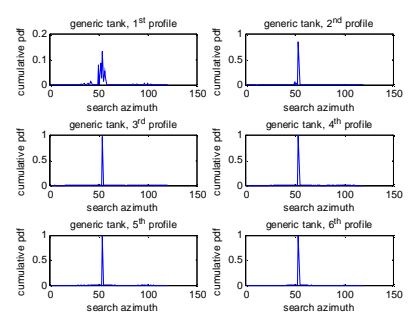Fig. 19 Discriminants

Fig. 20 Likelihoods

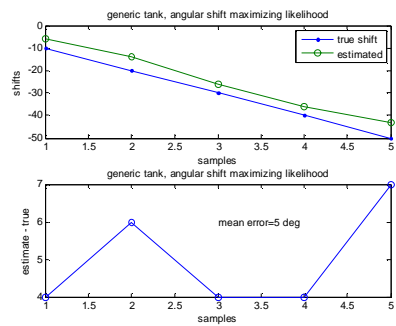Fig. 21 Cumulative PDF (Backward Combining)
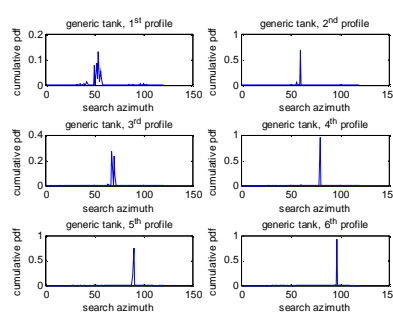

Fig. 22 Angular Shift per Sample (Turn Rate)

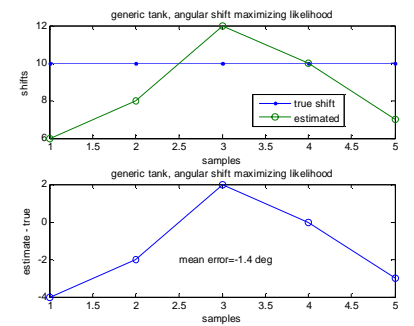Fig. 23 Cumulative PDF (Forward Combining)

Fig. 24 Angular Shift per Sample (Turn Rate)

Fig. 21 shows the cumulative PDF for backward combining, and similar to Fig. 15, it does become a point mass with probability one eventually.

Fig. 22 shows the estimated shifts vs. the true shifts, which develop a bias from the start as expected. The average angular error is 5 degrees.

Fig. 23 shows the cumulative PDF obtained using the template shifting (forward combining) and confusion matrix spreading. It is clear that after the confusion matrix spreading, the PDF does not amass at a single point as in Fig. 22.

954

Fig. 24 shows the estimated shifts vs. the true shifts. The average angular error is 1.5 degrees, which is a smaller angular bias in the turn rate estimation. This shows the advantage of using the forward combination over the backward one.

4 Conclusions

In this paper, the use of a minimum squared error-based classifier, namely, the MTE algorithm, for angular pose estimation was investigated. The local behavior of the classifier output was analyzed, leading to two estimation methods. The first method took the search angle that produces the smallest score as the pose estimate whereas the second method was based on the concept of likelihood function converted from the MTE classifier output. The likelihood function allowed for updating in a probabilistic manner, thus enabling angular tracking of targets that undergo maneuvers. Simulation results were presented to illustrate the operation and performance of these algorithms and methods.

The RF signatures used to create the range profiles via STARS in this paper were generated by SigPred as part of FATSO. As a public domain database, the target models of SigPred are of low-fidelity, which contains a lot of flat plates without much detail. This tends to make the response strong if viewed at the right angle but much weaker otherwise. The specific results presented in this paper may not be representative of a true target but the analysis remains valid. It is therefore interesting to apply the methods presented in this paper to similar target models created by a high-fidelity simulator such as Xpatch.

As the preliminary results for proof of concept, this paper considered favorable SNR conditions without clutter. More realistic scenarios with clutter are considered in [18] where targets near the clutter ridge need special attention. In addition to the development of pose-sensitive classifiers, it is of interest to investigate pose estimators based on robust nonlinear mappings from range profiles to pose angles. Once properly trained, a nonlinear mapping can be computationally more efficient than a template search and matching algorithm. Our ongoing effort is directed to these areas.

Acknowledgements

References

[1] C. Agate and K.J. Sullivan, "Road-Constraint Target Tracking and Identification Using a Particle Filter," in *Proc. of Signal and Data Processing of Small Targets* (O.E. Drummond, Ed.), Vol. 5204, 2003.

[2] E. Blasch, *Derivation of A Belief Filter for High Range Resolution Radar Simultaneous Target Tracking and Identification*, Ph.D. Dissertation, Wright State University, 1999.

[3] S.M. Herman, Joint Passive Radar Tracking and Target Classification Using Radar Cross Section, *Signal and Data Processing of Small Targets 2003* (Ed. By O.E. Drummond), Proc. of SPIE Vol. 5204.

[4] B.L. Johnson and T.P. Grayson, "Moving Target Exploitation," SPIE Conf. on Digitization of the Battlespace III (SPIE Vol. 3393), Orlando, FL, April 1998, 172-183

[5] V.I. Kaufman, T.D. Ross, E.M. Lavely, and E.P. Blasch, "Score-Based SAR ATR Performance Model with Operating Condition Dependencies," SPIE Defense and Security 2007: Sensor Data Exploitation and Target Recognition: Algorithms for Synthetic Aperture Radar Imagery XIV Conf., June 2007.

[6] J.R. Layne and D. Simon, A Multiple Model Estimator for A Tightly-Coupled HRR Automatic Target Recognition and MTI Tracking System, *SPIE Conf. on Algorithms for Synthetic Aperture Radar Imagery*, 1999.

[7] A.W. Learn, *Target Pose Estimation from Radar Data Using Adaptive Networks*, AFIT Master Thesis, March 1999.

[8] X.J. Liao, P. Runkle, and L. Carin, "Identification of Ground Targets from Sequential High Ranfe Resolution Radar Signatures," *IEEE Trans. on Aerospace and Electronic Systems*, 38-4, October 2002, 1230-1242.

[9] R.A. Mitchell and J.J. Westerkamp, "Robust Statistical Feature Based Air craft Identification," *IEEE Trans. on Aerospace and Electronic Systems*, 35-3, July 1999, 1077-1094.

[10] S.H. Musick, J.U. Sherwood, T.L. Piatt, N.A. Carlson, A Simulation System for Feature-Aided Tracking Research," *SPIE Defense & Security Symp.*, April 2004.

[11] J.C. Principe, D. Xu, and J. Fisher, Pose Estimation in SAR Using an Information Theoretic Criterion, *SPIE*, 3370: 218-29, 1998.

[12] T. L. Reinke, R. A. Mitchell, R. W. Hawley, A. Lindgren, M. Bartcsh, *Phase II: Radar Signature Exploitation During Move-Stop-Move Cycles,* Final Report, ATK Mission Research, 2005.

[13] K.J. Sullivan, M.B. Ressler, and R.L. Williams, "Signature-Aided Tracking Using HRR Profiles," SPIE, 2000.

[14] D. R. Wehner, *High Resolution Radar, Artech House*, Norwood, MA, 1987.

[15] R. Williams, J. Westerkamp, D. Gross, and A. Palomino, "Automatic Target Recognition of Time Crtical Moving Targets Using 1D High Range Resolution (HRR) Radar," *IEEE AES Systems Magazine*, April 2000, 37-43.

[16] C. Yang, M. Bakich, and E. Blasch, "Pose Angular-Aiding for Maneuvering Target Tracking," *Fusion'2005*, Philadelphia, PA, July 2005.

[17] C. Yang, Y. Bar-Shalom, and C.F. Lin, Discrete-Time Point Process Filter for Mode Estimation, *IEEE Trans. on Automatic Control*, 1992.

[18] C. Yang, E. Blasch, W. Garber, and R. Mitchell, "A Net Track Solution to Pose Angular Tracking of Maneuvering Targets in Clutter," *2007 Asilomar Conference on Signals, Systems and Computers*, Pacific Grove, CA, Nov. 2007.

[19] C. Yang, W. Garber, R. Mitchell, and E. Blasch, "A Simple Maneuver Indicator from Target's Range-Doppler Image," *Fusion'2007*, Quebec, Canada, July, 2007.